Hindawi Publishing Corporation
Journal of Nanomaterials
Volume 2013, Article ID 346274, 9 pages
http://dx.doi.org/10.1155/2013/346274

*Research Article*

# Fabrication of Gold Nanochains with Octreotide Acetate Template

**Jing Zhou,[1] Zhanzhao Fu,[2] Dawei Gao,[1] Faming Gao,[1] Na Li,[1] Xiaoning Zhao,[1] Yanping Liu,[1] Zi Wang,[1] and Guangxia Wang[2]**

[1] *Applying Chemistry Key Lab of Hebei Province, College of Environmental and Chemical Engineering, Yanshan University, No. 438 Hebei Street, Qinhuangdao 066004, China*
[2] *Oncology Department of Qinhuangdao First Hospital, No. 258 Wenhua Road, Qinhuangdao 066000, China*

Correspondence should be addressed to Dawei Gao; dwgao@ysu.edu.cn and Faming Gao; fmgao@ysu.edu.cn

Received 23 April 2013; Accepted 5 August 2013

Academic Editor: Xinqing Chen



We described a facile method for assembly gold nanochains by using octreotide acetate as template in aqueous environment. In acidic solution, octreotide acetate was conferred positive charges and its structure changed to chain-like. The monodisperse negative gold nanoparticles were bound to the surface of octreotide acetate template by electrostatic attraction and the interaction of gold nanoparticles with amino acid residues (tryptophan and lysine). The fabricated gold nanostructure presented chain-like observed by transmission electron microscopy. The cytotoxicity of gold nanochains was examined by tetrazolium dye-based microtitration (MTT) assay, which demonstrated significantly less toxicity than that of octreotide acetate alone. The MTT assay also reflected the combinative action between the gold nanoparticles with octreotide acetate. Our work lays the groundwork for developing octreotide acetate-templated nanomaterials that can be used as a building block for the creation of nanomaterials. Meanwhile, the harmfulless gold nanochains have great application prospects in the biomedical filed.

## 1. Introduction

Gold nanoparticles (AuNPs) have attracted increasing attention due to their great potential in biological and medical applications in recent years. AuNPs show excellent stability, universal biocompatibility, and unique optical, surface, electronic, and photocatalytic properties [1–4]. The biocompatibility and optical property have contributed to the increasing interest in utilizing AuNPs as optical markers for living cells [5], colorimetric sensors [6], contrast agent for optical coherence tomography imaging [7], and vehicles for drug and gene delivery [8]. The properties of AuNPs attribute to their surface plasmon resonance (SPR) property which is dependet upon their particle characteristics (shape and size) [9]. Many attempts have been made to control the shape and size for desirable functional properties during metal nanomaterials synthesis, such as photochemical method [10], electrochemical method [11], rapid microwave heating process [12], and liquid crystal template [13].

In various methods, biotemplate synthesis has emerged as an ideal encouraging approach to produce nanomaterials. The strategy can make AuNPs possessing excellent optical property by controlling the AuNPs at size and shape. Meanwhile, the biotemplate and AuNPs have high affinity, and the special morphologies of gold nanostructures were formed by different biotemplates. The high reproducibility and accuracy in controlling mineralizations and nanocrystal synthesis of various metals are also the merits of biotemplate method [14]. Therefore, various and wide range biomaterials as templates have become the focus for researchers. Griffin et al. [15] have made aqueous dispersion of DMAP-stabilized AuNPs adsorbed on the DNA template and achieved gold nanoscale wires. Zhang et al. [16] have prepared the periodic square-like AuNPs arrays functionalized with a layer of T15 sequences on 2D DNA nanogrids. Cowpea mosaic virus was modified with poly (allylamine) hydrochloride as template to form narrowly dispersed AuNPs [17]. However, all the chemical modification regents used in the preparation of AuNPs are

not desired. Meanwhile, whether the drug effect of AuNPs is affected by the biotemplate function did not get attention.

Therefore, we chose a neoteric strategy, using a new biomaterial as template to solve the problem of the chemical modifier. In numerous biomaterials, peptides have excellent potential as one of morphology-specific ligands due to their various amino acid sequences [18]. The morphology of the peptides can be controlled according to their physicochemical properties.

Octreotide acetate (OCT) is a synthetic octapeptide analogue of nature somatostatin [19], cyclized by a disulfide bond between the two Cys residues (D-Phe-c(Cys-Phe-D-Trp-Lys-Thr-Cys)-Thr(ol)) [20]. The amino acids composition of OCT is simple, and its physicochemical properties are available. To the best of our knowledge, using OCT as template to prepare gold nanochains has not been previously reported. The morphology and charges of OCT can be adjusted by experiment condition. In addition, OCT is a kind of medicine for the treatment of acromegaly, pancreatic endocrine tumors, and carcinoid syndrome [21]. The drug effect of template must be cleared away by our efforts so that the OCT-metal composite can be used in biomedicine without toxicity.

In this study, a mild, versatile, and controlled methodology was used to form OCT-AuNPs chains by assembling AuNPs with OCT. The morphology of OCT-AuNPs chains was characterized by TEM, and UV-vis spectroscopy was used to measure the optical property of OCT-AuNPs chains. Finally, 3-(4,5-dimethylazol-2-yl)-2,5-diphenyltetrazolium bromide (MTT) array was measured to evaluate whether the OCT-AuNPs chains have the drug toxic effect of OCT. The result of MTT array demonstrated the potential biomedicine applications of the obtained OCT-AuNPs chains. Meanwhile, the OCT-Au complex as contrast was also studied prepared by reducing the solution of Au (III) precursor and OCT.

## 2. Materials and Methods

*2.1. Materials.* Octreotide acetate ($C_{49}H_{66}N_{10}O_{10}S_2$) was purchased by Shanghai TASH Biotechnology Co., Ltd. (Shanghai, China). Gold (III) chloride ($AuCl_3$) was obtained from Chengdu West Chemical Co., Ltd. (Chengdu, China). Sodium borohydride ($NaBH_4$) was purchased from Tianjin chemistry factory (Tianjin, China). Hydrochloric acid (HCl) was supplied by Gu'an Chenmical plant (Langfang, China). 3-(4,5-dimeth-ylazol-2-yl)-2,5-diphenyltetrazolium bromide (MTT) got from Beyotime Institute of Biotechnology, Ltd. (Haimen, China). HeLa cells were provided by Cell Resource Center, IBMS, CAMS/PUMC. Deionized water prepared in our laboratory is used throughout all experiments.

*2.2. Preparation of OCT Biotemplate.* OCT powder (0.3 mg) was dissolved into 2 mL of 0.01 mM HCl at room temperature, in the dark. OCT was denatured and obtained positive charges owing to the acidic environment. Then, some bond sites of OCT were exposed so that its structure converted from microspheres to chains. Ultimately, OCT nanochains were prepared.

*2.3. Preparation of Monodisperse AuNPs.* The monodisperse AuNPs were synthesized by sodium borohydride reduction method at different Au : $NaBH_4$ molar ratios. The $AuCl_3$ (0.10, 0.25, 0.50, 0.75, and 1.00 mM, 1 mL), and freshly prepared $NaBH_4$ (253.0 mM, 100 $\mu$L) solutions were static for 1.5 min in ice bath and in the dark. Then, the $NaBH_4$ (253.0 mM, 10 $\mu$L) solution was separately pipetted into $AuCl_3$ solution with different concentration rapidly. Afterwards, the resultant solution was static for 4 min in ice bath. Finally, the yellow-brown monodisperse AuNPs solution was obtained.

*2.4. Preparation of OCT-AuNPs Chains.* OCT solution (200 $\mu$L) as prepared above was added to the disperse AuNPs solution. The solution changed color from yellow-brown to purple was observed promptly. The anionic AuNPs were allowed to adsorb onto the surface of the OCT nanochains with positive charges. The mixing solution was incubated for 5 min in the dark at room temperature. Ultimately, the OCT-AuNPs were prepared. The OCT at a pH of 8.0 was also studied.

*2.5. Preparation of OCT-Au Complex.* The OCT (0.15 mM, 200 $\mu$L) solution was mixed with light yellow $AuCl_3$ (5 mM, 200 $\mu$L), in incubation for 24 h. The long incubation time ensured Au ion combined with the template sufficiently. Then, the deposition appeared in the bottom of the tube. Ultimately following the OCT-$Au^{3+}$ was reduced with freshly prepared $NaBH_4$ (253.0 mM, 10 $\mu$L) solution, and the OCT-Au complex was obtained.

*2.6. Characterizations.* Transmission electron microscope (TEM) images were obtained on a Hitachi model H-7650 instrument operated at an accelerating voltage of 80 kV. The specimens were prepared for analysis by evaporating a drop of aqueous product onto a carbon-coated 300 mesh TEM copper grid and then naturally dried in air. The dates of AuNP size were calculated from TEM images using particle size distribution calculation software. The TEM instrument was used for presenting the crystal spacing of the OCT-AuNPs (0.5 mM) chains (HRTEM) at an accelerating voltage of 200 KV. Meanwhile, its crystallizations were further identified by the selected area electron-diffraction (SAED) pattern on a JEM model 2010 instrument. For investigating the component elements of the OCT-AuNPs (0.5 mM) chains, an energy-dispersive X-ray spectroscopy (EDS) equipped on the TEM was used.

UV-vis absorption spectra of the samples were recorded on a Shimadzu model UV-2550 double-monochromator spectrophotometer with 1 cm quartz cuvette. The spectra were collected over the range of 200–800 nm. To study the interaction between AuNPs and OCT template, the absorption spectra of monodisperse AuNPs and OCT were measured to compare with these of OCT-AuNPs chains. For the OCT-AuNPs chains analysis, the original concentrations of Au element were 0.10, 0.25, 0.5, 0.75, and 1.00 mM and the samples were diluted with deionized water (1 : 4).

*2.7. Cytotoxicity Determination by MTT Assay.* The human cervical carcinoma cell line (HeLa cell) was used to determine

the cytotoxicity of OCT-AuNPS chains (0.50 mM) by a tetrazolium dye-based microtitration (MTT) assay. Cells were cultured in Dulbecco's modified Eagle's medium (DMEM) containing fetal calf serum (10%) at 37°C in a 5% $CO_2$ incubator. Cells were plated out in 96-well plates at a density of 2000 cells per well in 200 $\mu$L and incubated for 24 h. Then, the cells were exposed to OCT-AuNPs with different dilution concentrations (initial concentration 0.25 mM, $10^{-1}$, $10^{-2}$, $10^{-3}$, $10^{-4}$, and $10^{-5}$) in 10 $\mu$L for 24 h, and OCT, AuNPs with the same concentration were used as control. Control cells were used without any sample treatment. MTT (0.012 mM, 10 $\mu$L) solution was added to each well, and the plates were incubated at 37°C for 4 h in the dark. The medium and MTT were then removed, and the MTT-formazan crystals were dissolved in 200 $\mu$L of DMSO. Then, the absorbance was measured at 560 nm using an enzyme-linked immunosorbent assay (ELLSA) reader. Each sample was performed independently in triplicate. All date were express as the mean ± SD. The cytotoxicity of OCT-AuNPs chains was calculated using the following formula:

$$\frac{\text{OD of treated cells} - \text{OD of background control}}{\text{OD of negative control} - \text{OD of background control}} \times 100\%. \quad (1)$$

*2.8. Statistical Analysis.* Dates are expressed as the mean and standard deviation (SD) in all experiments. Statistical analysis was performed using SPSS version 13.0. ANOVA was used to analyze statistical comparison between groups. The level of significance was set at $P < 0.01$.

## 3. Results and Discussion

*3.1. OCT-AuNPs Chains.* This procedure yielded AuNPs with different concentrations (1.0, 0.75, 0.5 mM) attached to the surface of the OCT scaffold was determined by TEM. Through the analysis of the particle size distribution calculation software, the mean AuNPs diameter and diameter distribution histogram were obtained. The dimensions of at least 200 AuNPs recorded on different locations of the TEM image have been compiled to obtain the date. Representative TEM images and the corresponding diameter distribution histograms of AuNPs were shown in Figure 1. TEM images showed that the structures of all the samples were apparent chain-like, and the AuNPs diameter was changed with the molar ratio of Au : $NaBH_4$. The average particle diameters of the OCT-AuNPs samples (0.5, 0.75, and 1.0 mM) are 4.18, 4.08, and 9.07 nm, respectively. The diameter of OCT-AuNPs sample (1.0 mM) is different with the others, and the range of particle diameter is wide from 2.44 nm to 28.74 nm, which is not what we expected. The reason leading to this result is that the high molar ratio of Au : $NaBH_4$ makes the $AuCl_3$ relative excess to $NaBH_4$, then $Au^{3+}$ cannot be reduced by $NaBH_4$ rapidly to form uniform particles. Conversely the reduced AuNPs provide seeds for the subsequent reduction of $AuCl_3$, and then the AuNPs diameter changed large. Interestingly, the Au contents of the OCT-AuNPs (0.1, 0.25 mM) samples were too low to form observed AuNPs on TEM.

The variation in surface morphology before and after the mix of the AuNPs and OCT biotemplate was also examined by TEM. Figure 2 showed the TEM images of monodisperse AuNPs (Figure 2(a)), OCT-AuNPs chains (Figure 2(b)). TEM images clearly indicated the morphology difference between the monodisperse AuNPs and OCT-AuNPs chains. The AuNPs had good dispersion without aggregation, and the OCT-AuNPs chains presented distinct chain-like morphology. The different morphological structure between AuNPs and OCT-AuNPs chains confirmed the monodisperse AuNPs were conjugated with OCT template to form nanochains. OCT changed the natural microsphere into branch chain at the pH 2.0, which provided the scaffold for the AuNPs assembling. It has been found that all the AuNPs are successfully combined with the OCT because of the clean background. On the contrary, Figure 2(c) shows that the phenomenon that AuNPs did not anchor to the surface of OCT template at alkaline environment (pH 8.0), despite that the OCT template presented ideal chain-like frame.

*3.2. Formation Mechanism of OCT-AuNPs Chains.* OCT is a synthetic octapeptide analogue of nature somatostatin, cyclized by a disulfide bond between the two Cys residues (D-Phe-c(Cys-Phe-D-Trp-Lys-Thr-Cys)-Thr(ol)). OCT is a charged molecule, containing nonpolar amino acids (Phe, Trp), polar uncharged amino acids (Cys, Thr), and alkaline amino acid (Lys). In aqueous solution, OCT is ionized to form zwitterions. So, we can control the electronic charges of OCT by adjusting the pH of solution. According the report that OCT exhibits a net $2^+$ charge at pH 5.5 [21], and OCT presents positive charges at pH 2.0 evidently. The surface of monodisperse AuNPs conjugates covering layer of $AuCl^{2-}$, which makes AuNPs show negative charges. The negative charges of the AuNPs exclude mutually to form a passivating on the surface. Then, the passivating makes AuNPs possess good dispersion. Accompanying the mixing between OCT and AuNPs, AuNPs bound to the surface of OCT by electrostatic force. In the meantime, AuNPs could not absorb on the negatively charged OCT template at pH 8.0, which also proved that the combination of AuNPs and OCT by electrostatic interaction at acid environment on the opposite.

In addition, Tan et al. has reported that all the amino acids have different capping capability for the AuNPs. There are many other reports mentioned AuNPs can interact with many amino acid residues, such as tyrosine [22], lysine, cysteine, histidine [14], and aspartic acid [23]. Hence, the amino acid residues on the OCT can be used as capping agents to form OCT-AuNPs chains.

*3.3. OCT-Au Complex.* Preparation of OCT-Au complex as the control experiment was researched. The TEM image (Figure 3) showed that the OCT-Au complex presented serious agglomeration and its morphology offered a depressing picture. Many reports have put forward the preparation methods: incubation of the biomaterials with Au (III) solution was reduced by reducing regent. However, we found the structures of the biomaterials used as templates in the literature were pretty stable and constant, such as DNA [24],

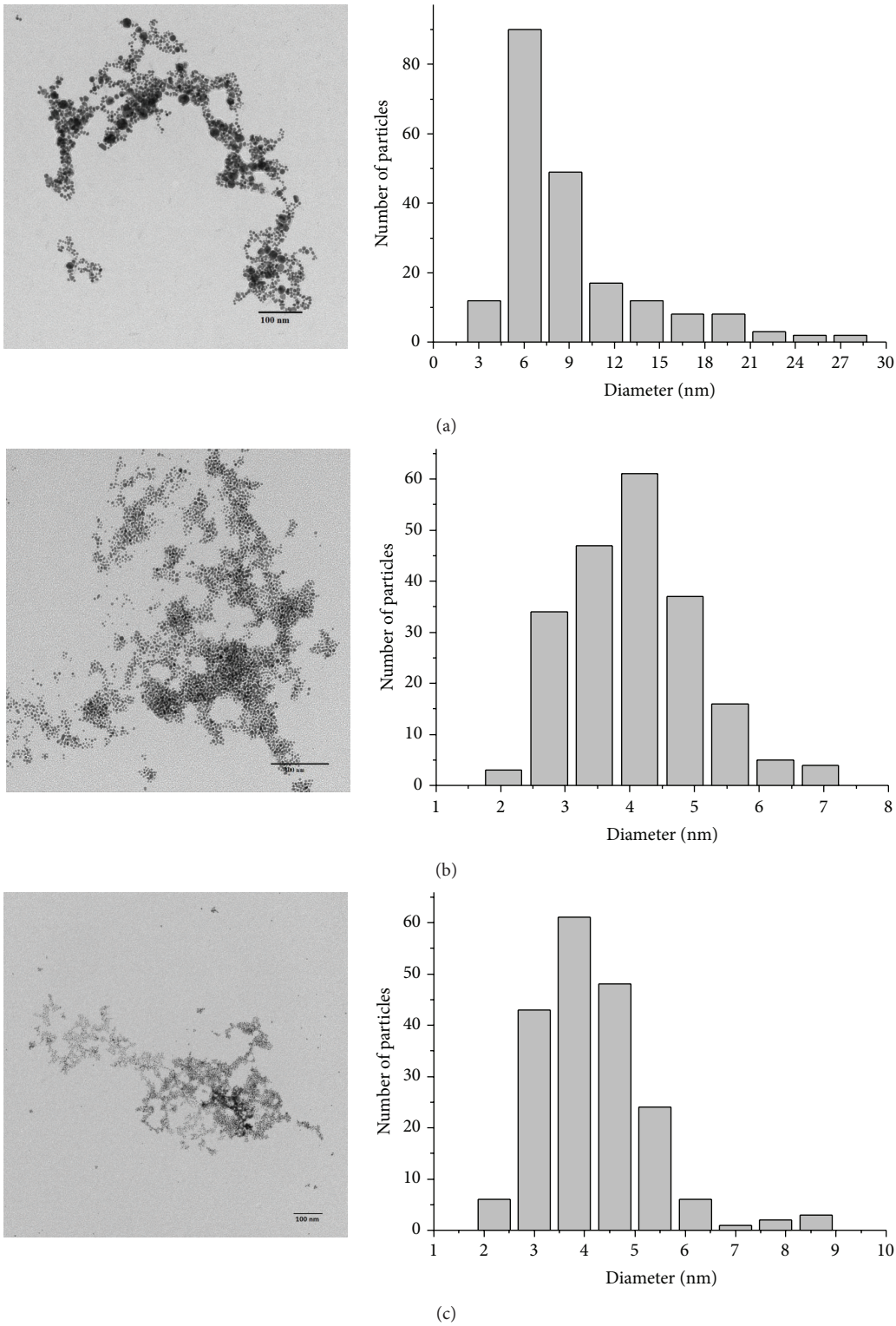


Figure 1: Representative TEM images (left) and the corresponding diameter distribution hist-ograms (right) of OCT-AuNPs chains with different concentrations: (a) 1.0, (b) 0.75, and (c) 0.5 mM.

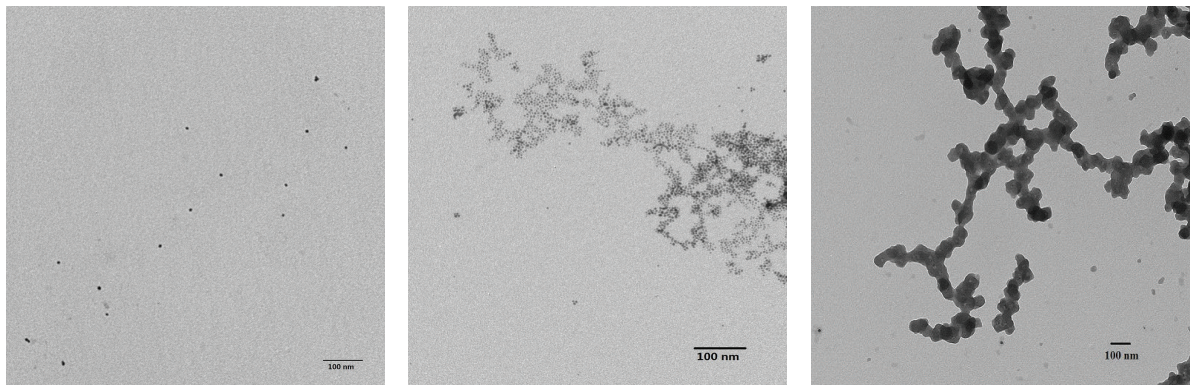


(a) (b) (c)

Figure 2: TEM images of dispersion AuNPs (a), before and after mixed with OCT template at pH 2.0 (b), and pH 8.0 (c).

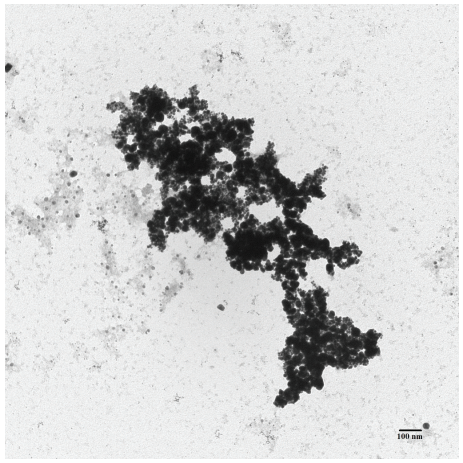


Figure 3: TEM image of OCT-Au complex prepared by the co-incubation of OCT and $AuCl_3$.

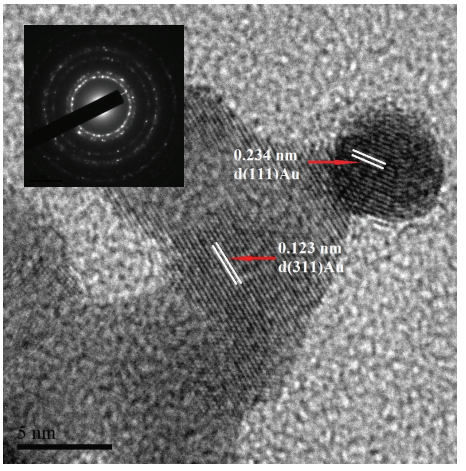


Figure 4: HRTEM image of OCT-AuNPs (0.50 mM) chains, and the inset image shows the SAED pattern, corresponding to (111), (200), (220), (311), and (222) planes of Au fcc crystals.

virus [25], and CNTs modified with peptide [14]. This made these materials endure nasty drastic regents. The reason for such frustrated image may be that the effect of the reducing regent ($NaBH_4$) on OCT changes its structure.

There has been reported some amino acids including Try own reductive capability [26], which may also lead to the despairing result.

*3.4. Microstructure and Compose of OCT-AuNPs Chains.* The microstructure of AuNPs (0.5 mM) absorbing on the OCT nanochains was checked by HRTEM technique. The HRTEM image (Figure 4) exhibited clear fringes with spacings of 0.234 and 0.123 nm, which agrees well with the {111} and {311} lattice planes in face-centered cubic (fcc) Au. The good lattice structure was future confirmed by the corresponding selected-area electron diffraction (SAED) pattern given in the inset of Figure 4. SAED pattern of AuNPs was similar with Figure 1(D) of literature [27], showing the ring patterns with intense spots assigned to (111), (200), (220), (311), and (222) planes of Au fcc crystals. Both the HRTEM image and SAED pattern confirmed that the prepared AuNPs displayed in the form of polycrystalline state and structurally uniform.

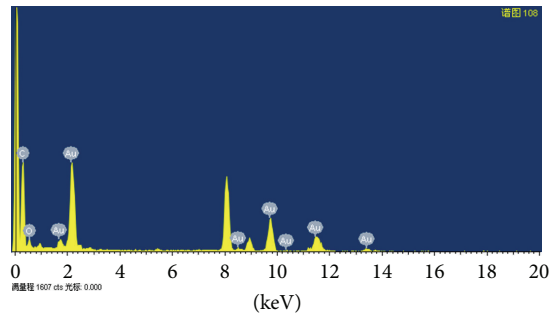


Figure 5: EDX analysis of OCT-AuNPs (0.50 mM) chains.

The composition of OCT-AuNPs chains (0.5 mM) was analyzed by energy-dispersive X-ray spectroscopy (EDS). A typical EDS spectrum was shown in Figure 5. The appearance of various prominent peaks of gold confirmed the presence of gold element. The C signal arose from the carbon-coated copper grid and the OCT peptide. The presence of oxygen was attributed to the OCT peptide and water adsorbed on the

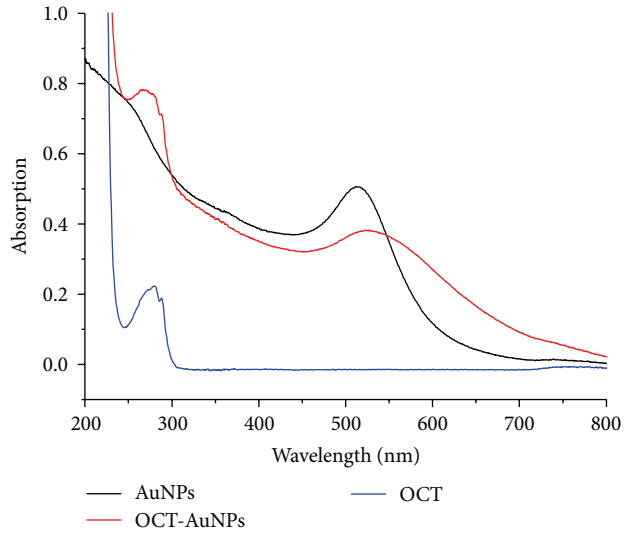


Figure 6: UV-vis spectra of OCT, AuNPs, and OCT-AuNPs chains.

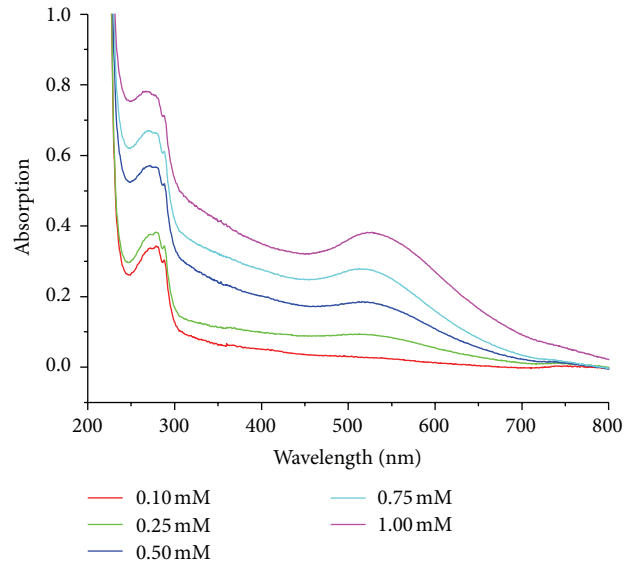


Figure 7: UV-vis spectra of OCT-AuNPs chains with different concentrations.

grid. Besides the Cu peaks coming from the copper grid were removed. Finally, the EDS spectrum confirmed that the OCT-AuNPs chains contained gold, carbon, and oxygen elements.

*3.5. UV-Vis Spectrophotometry of OCT-AuNPs Chains.* To confirm the interaction of OCT and AuNPs, the UV-Vis absorption spectra of OCT, AuNPs, and OCT-AuNPs were shown in Figure 6. In Surujpaul's research, the UV-vis spectrophotometry of the [$Tyr^3$] octreotide protected with Boc was reported, the absorption peak wavelengths of TOC-Boc were at 278, 289, and 273 nm [28]. In our study, the OCT peptide showed an absorption spectrum with maximum of 279 nm and defined negative peak at 289 nm pertaining to the phenyl groups of tryptophan residue. Our results are basic consistent with that of the literature except the peak wavelength at 273 nm causing by $Tyr^3$ residue. The UV-vis spectrum of monodisperse AuNPs was at 512 nm between 500~600 nm, assigned to the surface plasmon resonance of small AuNPs [29]. Compared with the spectra of OCT and AuNPs, the absorption spectra of OCT-AuNPs chains appeared evident wavelength shift, which can be attributed to the AuNPs binding to Try residue. Therefore, the conclusion of AuNPs adsorbed onto the surface of OCT can be proved.

The UV-Vis absorption spectra of OCT-AuNPs chains with different concentrations are presented in Figure 7. The spectra absorbance increased as the increase of AuNPs concentration. The samples of high gold concentrations showed two dominant absorption peaks: the absorption peak of OCT at above 270 nm and the SPR peak of AuNPs around 520 nm. No absorption of the samples with low gold contents can be observed in the 520 nm region due to the development of surface plasmon band. This is consistent with many literature reports of the absences of the surface plasmon band for AuNPs of diameter less than 2 nm [30].

On the other hand, the AuNPs absorption peaks displayed red shift along with the increase of concentrations in general except the sample (0.75 mM). The phenomenon is relative to the SPR of AuNPs. The AuNPs with different particle diameters produced different SPR effects, leading to the red shift in the absorption peak. The mean diameter of sample (0.75 mM) is slightly smaller than that of the sample (0.5 mM), so the sample (0.75 mM) became a special case. The special case also proved the theory that the surface plasmon resonance (SPR) property of AuNPs depended upon their particle characteristics (shape and size) [31, 32]. In addition, there was an evident color-changing phenomenon accompanying with the increase of gold concentrations. Figure 8 showed the color-changing of the monodisperse AuNPs (Figure 8(a)) and OCT-AuNPs chains (Figure 8(b)). The colors of the solutions were darkened from right to left in sequence. The color distinction of AuNPs and OCT-AuNPs chains also testified that AuNPs and OCT had interacted with each other at the same time.

*3.6. Cytotoxicity of OCT-AuNPs Chains.* Just like other drugs, OCT has some side effects, including nausea, vomiting, loose/oily stools, and constipation. OCT-AuNPs chains need to be examined for biocompatibility if they are to be manufactured on a large scale for *in vivo* usage. So, we used the MTT assay and HeLa cell lines to detect their drug toxic effect. The OCT and AuNPs as control were also subjected to the MTT assay for cytotoxicity estimate at the same dose. The bar histogram of MTT assay result (Figure 9) performed the cell viability at different sample concentrations, and the statistical analysis showed there is significant difference ($P < 0.01$). At each concentration, the cell viability degrees of OCT, OCT-AuNPs chains, and AuNPs were increased successively. The AuNPs possessed the highest cell viability, so we compared all the MTT results with AuNPs at the corresponding concentration. From the histogram, we can know that the cell viability of OCT-AuNPs chains was much higher than that of OCT and was similar to the AuNPs (except

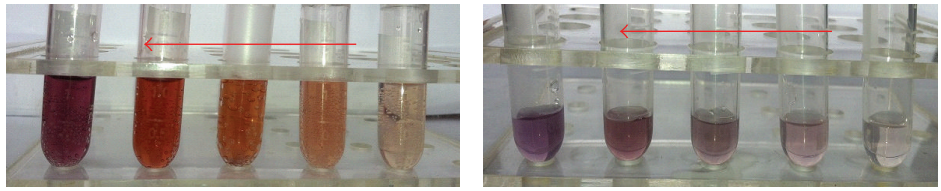

(a) (b)

Figure 8: Pictures of dispersion AuNPs solutions (a) and OCT-AuNPs solutions (b) with different concentrations. The concentration increased from left to right: 0.10, 0.25, 0.50, 0.75, 1.00 mM.

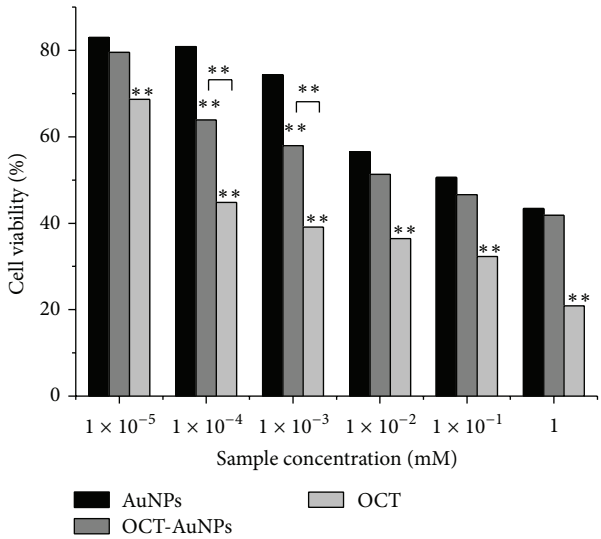


Figure 9: Cytotoxicity of the monodisperse AuNPs, octreotide acetate (OCT), and OCT-AuNPs chains study by MTT assay. HeLa cells were incubated with samples with different concentrations (initial concentrations 1 = 0.25 mM), $^{**}P < 0.01$ compared with AuNPs.

$0.25 \times 10^{-3}$, $10^{-4}$ mM). For example, the cell viability of OCT-AuNPs chains ($0.25 \times 10^{-5}$) was up to 79.57%, which accessed to the AuNPs' cell viability (82.98%). But, the OCT resulted in nearly 40% loss of cell viability. The statistical analysis also proved the conclusion that the significant differences were observed between OCT template and OCT-AuNPs/AuNPs. The cell viability of OCT ($0.25 \times 10^{-3}$, $10^{-4}$ mM) samples only had slight change compared with the OCT sample ($0.25 \times 10^{-2}$ mM) ($P > 0.05$); nevertheless, the cell viability of AuNPs in different concentrations have been apparently elevated. These indicated that OCT-AuNPs chains had not the complete toxic effect of OCT. It is well known that the AuNPs have good biocompatibility [33], then we analyzed the phenomenon that biocompatibility of AuNPs we prepared was lower than to other reports. Shukla and his research group used dialysis to remove excess free borohydride ions and unreduced chloroaurate ions presented in the gold solution [34], but we did not do the dialysis procedure in our work. The previous reports have shown Au (III) ions bind strongly to DNA and nervous systems [35, 36]. Then, our prepared gold nanochains possessed slight toxicity might be accounted for the AuNPs/OCT-AuNPs solutions contained free borohydride ions and unreduced chloroaurate ions.

OCT-AuNPs chains with lower toxicity than OCT can attribute the success to the interaction of AuNPs with the biological active sites of OCT. The essential amino acids of OCT are Phe3, Trp4, Lys5, and Thr6, in which Lys is the key active site of OCT peptide [27]. Lys, one kind of alkaline amino, brings positive charges at acidic environment. AuNPs bound with these amino residues, which resulted in the part extermination of OCT toxic effect following. Therefore the MTT assay proved that AuNPs adsorbed onto the surface of OCT, which coincided with the above mentioned mechanism.

## 4. Conclusion

In summary, we have successfully demonstrated that octreotide acetate as biotemplate was used to assemble gold nanochains in aqueous environment for the first time. The significant findings include that a unique aspect of octreotide acetate is the ability to change its morphology to chain-like by adjusting pH value, which makes it attractive scaffolds for ordered arrays of nanochains. The formation mechanism of gold nanochains can be summarized as the electrostatic interaction between octreotide acetate and gold nanoparticles, conjugation of gold with special amino acids, Trp, and Lys. The [$NaBH_4$] to [$AuCl_3$] ratio determined the diameter of gold nanoparticles to change their surface plasmon resonance effects. The resulting OCT-AuNPs chains can have upstanding biomedicine applications because they did not have the evident toxic effect of octreotide acetate.

## Authors' Contribution

Jing Zhou and Zhanzhao Fu have equally contributed to this paper.

## Acknowledgment

This work was financially supported by a research grant from the Chinese Ministry of Education Doctor Degree (20101333120011), grants from the Hebei Province Natural Science Fund (C2011203137, 11965152D), and a Chinese postdoctoral grant (480013).

## References

[1] Z. Krpetić, P. Nativo, F. Porta, and M. Brust, "A multidentate peptide for stabilization and facile bioconjugation of gold

Nanoparticles," *Bioconjugate Chemistry*, vol. 20, no. 3, pp. 619–624, 2009.

[2] H. Jaganathan and A. Ivanisevic, "In vivo molecular probing of cellular ompartments with gold nanoparticles and nanoaggregates," *ACS Applied Materials & Interfaces*, vol. 2, no. 5, pp. 1407–1413, 2010.

[3] A. Housni, M. Ahmed, S. Liu, and R. Narain, "Monodisperse protein stabilized gold nanoparticles via a simple photochemical process," *The Journal of Physical Chemistry C*, vol. 112, no. 32, pp. 12282–12290, 2008.

[4] T. Jiao, Y. Wang, W. Guo et al., "Synthesis and photocatalytic property of gold nano- particles by using a series of bolaform Schiff base amphiphiles," *Materials Research Bulletin*, vol. 47, no. 12, pp. 4203–4209, 2012.

[5] H. Ba, J. Rodríguez-Fernández, F. D. Stefani, and J. Feldmann, "Immobilization of gold nanoparticles on living cell membranes upon controlled lipid binding," *Nano Letters*, vol. 10, no. 8, pp. 3006–3012, 2010.

[6] M. E. Ali, S. Mustafa, Y. B. Che Man, and K. N. Islam, "Gold nanoparticle sensor for the visual detection of pork adulteration in meatball formulation," *Journal of Nanomaterials*, vol. 2012, Article ID 103607, 7 pages, 2012.

[7] Y. Ponce de León, J. L. Pichardo-Molina, N. Alcalá Ochoa, and D. Luna-Moreno, "Contrast enhan- cement of optical coherence tomography images using branched gold nanoparticles," *Journal of Nanomaterials*, vol. 2012, Article ID 571015, 9 pages, 2012.

[8] M. A. Colleen, C. D. James, and M. M. Mathew, "Investigation of the drug binding properties and cytotoxicity of DNA-capped nanoparticles designed as delivery vehicles for the anticancer doxorubicin and actinomycin D," *Bioconjugate Chemistry*, vol. 23, no. 10, pp. 2061–2070, 2012.

[9] J. Nam, N. Won, H. Jin, H. Chung, and S. Kim, "pH-induced aggregation of gold nanoparticles for photothermal cancer therapy," *Journal of the American Chemical Society*, vol. 131, no. 38, pp. 13639–13645, 2009.

[10] K. Matsuda, H. Yamaguchi, T. Sakano, M. Ikeda, N. Tanifuji, and M. Irie, "Conductance photoswitching of diarylethene-gold nanoparticle network induced by photochromic reaction," *The Journal of Physical Chemistry C*, vol. 112, no. 43, pp. 17005–17010, 2008.

[11] M. Zhou, S. Chen, S. Zhao, and H. Ma, "Preparation of gold nanoplates by an electrochemical method," *Chemistry Letters*, vol. 34, no. 12, pp. 1670–1671, 2005.

[12] S. K. Seol, D. Kim, S. Jung, W. S. Chang, and J. T. Kim, "One-step synthesis of PEG-coated gold nanoparticles by rapid microwave heating," *Journal of Nanomaterials*, vol. 2013, Article ID 531760, 6 pages, 2013.

[13] M. Yamamoto, Y. Kashiwagi, T. Sakata, H. Mori, and M. Nakamoto, "Synthesis and morphology of star-shaped gold nanoplates protected by poly(N-vinyl-2-pyrrolidone)," *Chemistry of Materials*, vol. 17, no. 22, pp. 5391–5393, 2005.

[14] R. Djalali, Y.-F. Chen, and H. Matsui, "Au nanocrystal growth on nanotubes controlled by conformations and charges of sequenced peptide templates," *Journal of the American Chemical Society*, vol. 125, no. 19, pp. 5873–5879, 2003.

[15] F. Griffin, A. Ongaro, and D. Fitzmaurice, "DNA-templated assembly of nanoscale wires and protein-functionalized nanogap contacts," *Analyst*, vol. 129, no. 12, pp. 1171–1175, 2004.

[16] J. Zhang, Y. Liu, Y. Ke, and H. Yan, "Periodic square-like gold nanoparticle arrays templated by self-assembled 2D DNA nanogrids on a surface," *Nano Letters*, vol. 6, no. 2, pp. 248–251, 2006.

[17] A. A. A. Aljabali, G. P. Lomonossoff, and D. J. Evans, "CPMV-polyelectrolyte-templated gold nanoparticles," *Biomacromolecules*, vol. 12, no. 7, pp. 2723–2728, 2011.

[18] L. M. Forbes, A. P. Goodwin, and J. N. Cha, "Tunable size and shape control of platinum nanocrystals from a single peptide sequence," *Chemistry of Materials*, vol. 22, no. 24, pp. 6524–6528, 2010.

[19] Y. Iwase and Y. Maitani, "Octreotide-targeted liposomes loaded with CPT-11 enhanced cytotoxicity for the treatment of medullary thyroid carcinoma," *Molecular Pharmaceutics*, vol. 8, no. 2, pp. 330–337, 2011.

[20] H. M. Bigott-Hennkens, S. Junnotula, L. Ma, F. Gallazzi, M. R. Lewis, and S. S. Jurisson, "Synthesis and in vitro evaluation of a rhenium-cyclized somatostatin derivative series," *Journal of Medicinal Chemistry*, vol. 51, no. 5, pp. 1223–1230, 2008.

[21] D. T.-W. Lau, J. W. Sharkey, L. Petryk, F. A. Mancuso, Z. Yu, and F. L. S. Tse, "Effect of current magnitude and drug concentration on iontophoretic delivery of octreotide acetate (Sandostatin) in the rabbit," *Pharmaceutical Research*, vol. 11, no. 12, pp. 1742–1746, 1994.

[22] D. Toroz and S. Corni, "Peptide synthesis of gold nanoparticles: the early steps of gold reduction investigated by density functional theory," *Nano Letters*, vol. 11, no. 3, pp. 1313–1318, 2011.

[23] Y. N. Tan, J. Y. Lee, and D. I. C. Wang, "Aspartic acid synthesis of crystalline gold nanoplates, nanoribbons, and nanowires in aqueous solutions," *The Journal of Physical Chemistry C*, vol. 112, no. 14, pp. 5463–5470, 2008.

[24] C. M. Niemeyer and U. Simon, "DNA-based assembly of metal nanoparticles," *European Journal of Inorganic Chemistry*, no. 18, pp. 3641–3655, 2005.

[25] C. Radloff, R. A. Vaia, J. Brunton, G. T. Bouwer, and V. K. Ward, "Metal nanoshell assembly on a virus bioscaffold," *Nano Letters*, vol. 5, no. 6, pp. 1187–1191, 2005.

[26] Y. N. Tan, J. Y. Lee, and D. I. C. Wang, "Uncovering the design rules for peptide synthesis of metal nanoparticles," *Journal of the American Chemical Society*, vol. 132, no. 16, pp. 5677–5686, 2010.

[27] L. Kemal, X. C. Jiang, K. Wong, and A. B. Yu, "Experiment and theoretical study of poly(vinyl pyrrolidone)-controlled gold nanoparticles," *The Journal of Physical Chemistry C*, vol. 112, no. 40, pp. 15656–15664, 2008.

[28] P. P. Surujpaul, C. Gutiérrez-Wing, B. Ocampo-García et al., "Gold nanoparticles conjugated to [Tyr3]Octreotide peptide," *Biophysical Chemistry*, vol. 138, no. 3, pp. 83–90, 2008.

[29] M. Filali, M. A. R. Meier, U. S. Schubert, and J.-F. Gohy, "Star-block copolymers as templates for the preparation of stable gold nanoparticles," *Langmuir*, vol. 21, no. 17, pp. 7995–8000, 2005.

[30] J. Majimel, D. Bacinello, E. Durand, F. Vallée, and M. Tréguer-Delapierre, "Synthesis of hybrid gold-gold sulfide colloidal particles," *Langmuir*, vol. 24, no. 8, pp. 4289–4294, 2008.

[31] K. L. Kelly, E. Coronado, L. L. Zhao, and G. C. Schatz, "The optical properties of metal nanoparticles: the influence of size, shape, and dielectric environment," *The Journal of Physical Chemistry B*, vol. 107, no. 3, pp. 668–677, 2003.

[32] G. Wang and W. Sun, "Optical limiting of Gold nanoparticle aggregates induced by electrolytes," *The Journal of Physical Chemistry B*, vol. 110, no. 42, pp. 20901–20905, 2006.

[33] N. Lewinski, V. Colvin, and R. Drezek, "Cytotoxicity of nanopartides," *Small*, vol. 4, no. 1, pp. 26–49, 2008.

[34] R. Shukla, V. Bansal, M. Chaudhary, A. Basu, R. R. Bhonde, and M. Sastry, "Biocompatibility of gold nanoparticles and their endocytotic fate inside the cellular compartment: a microscopic overview," *Langmuir*, vol. 21, no. 23, pp. 10644–10654, 2005.

[35] Y.-K. Yang, S. Lee, and J. Tae, "A goid(III) ion-Selective fluorescent probe and its application to bioimagings," *Organic Letters*, vol. 11, no. 24, pp. 5610–5613, 2009.

[36] E. Nyarko, T. Hara, D. J. Grab et al., "In vitro toxicity of palladium(II) and gold(III) porphyrins and their aqueous metal ion counterparts on Trypanosoma brucei brucei growth," *Chemico-Biological Interactions*, vol. 148, no. 1-2, pp. 19–25, 2004.